# Tanycytes control hypothalamic liraglutide uptake and its anti-obesity actions

Monica Imbernon, Chiara Saponaro, Hans Christian Cederberg Helms, Manon Duquenne, Daniela Fernandois, Eleonora Deligia, Raphael G.P. Denis, Daniela Herrera Moro Chao, Sowmyalakshmi Rasika, Bart Staels, et al.

Published in final edited form as:
*Cell Metab*. 2022 July 05; 34(7): 1054–1063.e7. doi:10.1016/j.cmet.2022.06.002.

# Tanycytes Control Hypothalamic Liraglutide Uptake and its Anti-Obesity Actions

**Monica Imbernon**[#1], **Chiara Saponaro**[#2], **Hans Christian Cederberg Helms**[1,3], **Manon Duquenne**[1], **Daniela Fernandois**[1], **Eleonora Deligia**[1], **Raphael G.P. Denis**[4], **Daniela Herrera Moro Chao**[4], **S. Rasika**[1], **Bart Staels**[5], **François Pattou**[2], **Frank W. Pfrieger**[6], **Birger Brodin**[3], **Serge Luquet**[4], **Caroline Bonner**[#2,*], **Vincent Prevot**[#1,8,*]

[1]Univ. Lille, Inserm, CHU Lille, Laboratory of Development and Plasticity of the Neuroendocrine Brain, Lille Neuroscience & Cognition, UMR-S 1172, European Genomic Institute for Diabetes (EGID), F-59000 Lille, France

[2]Univ. Lille, CHU Lille, Inserm U1190, EGID, Institut Pasteur de Lille, F-59000 Lille, France

[3]Department of Pharmacy, University of Copenhagen, Copenhagen-2100, Denmark

[4]Université de Paris, BFA, UMR 8251, CNRS, F-75013 Paris, France

[5]Univ. Lille, Inserm, CHU Lille, Institut Pasteur de Lille, U1011-EGID, Lille, France

[6]Centre National de la Recherche Scientifique, Université de Strasbourg, Institut des Neurosciences Cellulaires et Intégratives, Strasbourg, France

[#] These authors contributed equally to this work.

## Summary

Liraglutide, an anti-diabetic drug and agonist of the glucagon-like peptide 1 receptor (GLP1R), has recently been approved to treat obesity in individuals with or without type-2 diabetes. Despite its extensive metabolic benefits, the mechanism and site of action of liraglutide remain unclear. Here, we demonstrate that liraglutide is shuttled to target cells in the mouse hypothalamus by specialized ependymoglial cells called tanycytes, bypassing the blood-brain barrier. Selectively silencing GLP1R in tanycytes or inhibiting tanycytic transcytosis by botulinum neurotoxin expression not only hampers liraglutide transport into the brain and its activation of target hypothalamic neurons, but also blocks its anti-obesity effects on food intake, body weight and fat mass, and fatty acid oxidation. Collectively, these striking data indicate that the liraglutide-induced activation of hypothalamic neurons and its downstream metabolic effects are mediated by its

[*]***Corresponding authors:*** Vincent Prevot (vincent.prevot@inserm.fr; +33 612-90-38-76) and Caroline Bonner (caroline.bonner@univ-lille.fr; +33 651-58-32-70).
[8]Lead contact

**Author Contributions**

M.I. and V.P. conceived the study. M.I., C.S., H.C.C.H., M.D., D.F,. E.D., carried out the experiments. H.C.C.H. and B.B. set up the classical BBB model and performed *in vitro* barrier experiments. M.I., R.G.P.D.n D.H.M.C. and S.L. conducted metabolic phenotyping. D.F. and M.I. performed microdialysis experiments. F.W.P. generated the iBot animal model. M.I., C.S., B.S., F.P., S.L., C.B. and V.P. designed and planned the experiments. M.I., C.S., C.B. and V.P. wrote the paper. S.R. edited the manuscript. All authors contributed to the preparation of the manuscript.

**Declaration Of Interests**

The authors declare no competing interests.


Europe PMC Funders Author Manuscripts

Europe PMC Funders Author Manuscripts

tanycytic transport into the mediobasal hypothalamus, strengthening the notion of tanycytes as key regulators of metabolic homeostasis.

## Abstract

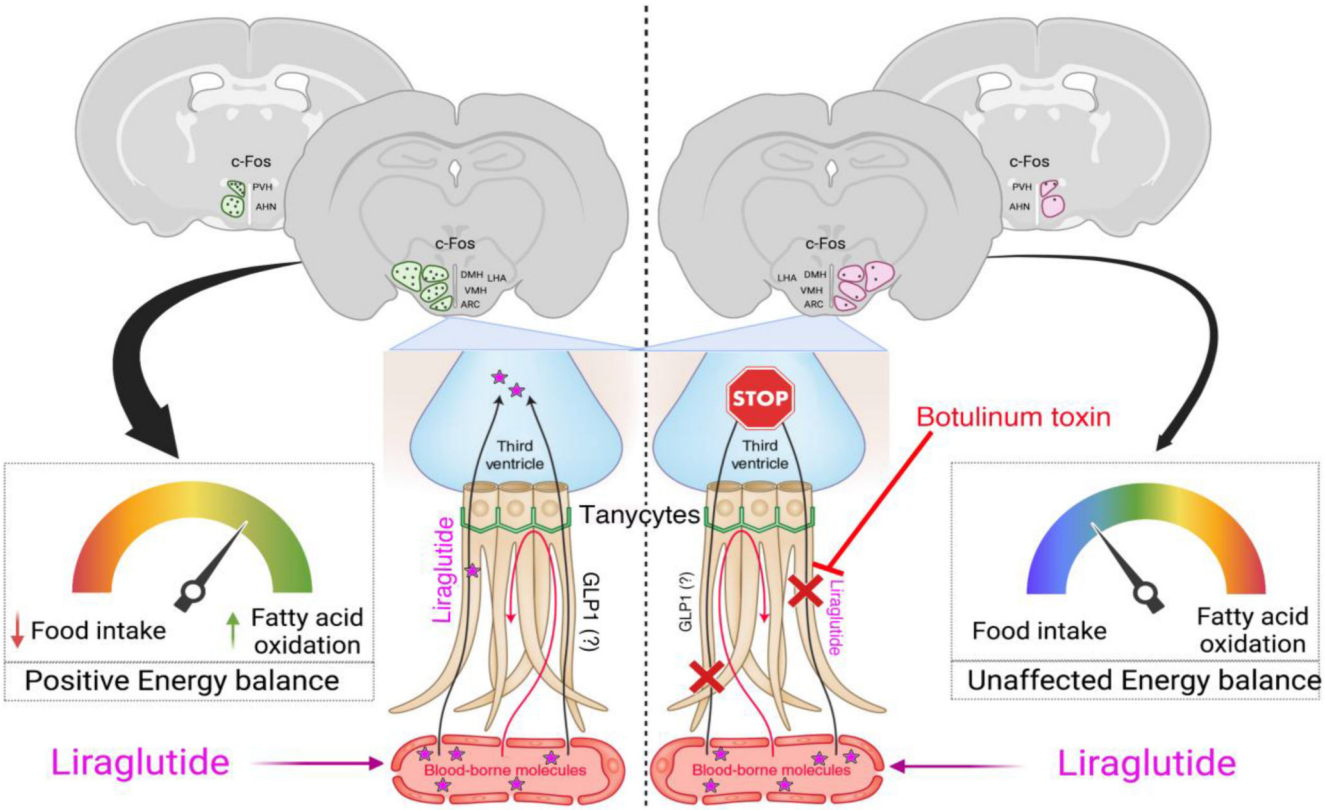


## Introduction

Glucagon-like peptide 1 (GLP1; 7–36 amide), an incretin hormone mainly secreted by intestinal L-cells in response to glucose and other ingested nutrients, induces insulin secretion via its receptor, GLP1R, in a glucose-regulated manner (Kjems et al., 2003; Peyot et al., 2009). GLP1 is also endogenously produced in several metabolic organs including pancreatic alpha cells (Chambers et al., 2017) and neurons of the nucleus of the solitary tract (NTS), which mainly project to the hypothalamus (Holt et al., 2019). However, the rapid degradation of native GLP1 by dipeptidyl peptidase 4 (DPP-4) *in vivo* limits its therapeutic potential. This has led to the development of GLP1R agonists with a longer half-life that promote a wide range of benefits including reduced food intake, increased weight loss and improved glycemic control, and some of these agonists have been approved by American and European health agencies for the treatment of obesity and type-2 diabetes (T2D) (Drucker et al., 2017). The GLP1R agonist liraglutide has an amino acid sequence that is 97% identical to that of human GLP1 and carries an additional albumin-binding fatty-acid side-chain (Garber, 2011) that reduces its cleavage by DPP-4 and prolongs its half-life when compared to endogenous GLP1 (Kim and Egan, 2008). Among its various

metabolic effects, liraglutide reduces food intake and body weight, leading to its recent approval as an anti-obesity treatment for individuals with or without T2D (Drucker et al., 2017).

Extensive studies have shown that liraglutide regulates energy homeostasis by acting via the central nervous system (CNS), particularly the hypothalamus (Adams et al., 2018; Beiroa et al., 2014; Secher et al., 2014; Sisley et al., 2014; Timper et al., 2020) and the brainstem (Fortin et al., 2020). Initially, liraglutide was thought to reach target cells in the mediobasal hypothalamus that regulate metabolism by crossing the blood-brain barrier (BBB) either at the level of microvessels or at circumventricular organs (CVOs) such as the median eminence (ME) or the area postrema (AP), which lie adjacent to the arcuate nucleus of the hypothalamus (ARH) (Banks, 2019; Mullier et al., 2010; Prevot et al., 2018), and the nucleus of the solitary tract (Fortin et al., 2020), respectively. However, its exact route of transport into these areas remains unknown. A recent study in which the AP was surgically resected suggests that this CVO is not required for the brain-mediated effects of liraglutide on food intake and body weight (Fortin et al., 2020). On the other hand, in the ME, highly specialized ependymoglial cells called tanycytes transport blood-borne metabolic signals such as leptin and ghrelin into the cerebrospinal fluid (CSF), thus acting as gatekeepers for these molecules (Balland et al., 2014; Collden et al., 2015; Duquenne et al., 2021; Garcia-Caceres et al., 2019; Prevot et al., 2018). Due to the privileged position of ME tanycytes, which are in direct contact with blood-borne nutrients and hormones through the fenestrated endothelial walls of ME capillaries (Langlet et al., 2013b), we hypothesized that these cells could also mediate the entry of liraglutide into the mediobasal hypothalamus, enabling it to regulate energy homeostasis.

## Results

### Blood-borne liraglutide is transported by tanycytes into the median eminence

In order to “catch” liraglutide in the process of entering the brain and thereby determine its route of access, we fluorescently labeled liraglutide and administered it intravenously through the jugular vein. We observed that 60 seconds after its injection, liraglutide did not cross the microvascular endothelial cells of the BBB (Fig. 1a, yellow arrows), but extravasated through the fenestrated vessels of the ME. Its presence in tanycytes and neuronal cell bodies of the ventromedial ARH (vmARH) at this short time point suggests uptake by a direct action on cells lying outside the BBB (Fig. 1a). Furthermore, in an *in vitro* model of the BBB (Supplementary Fig. 1a-c) (Helms and Brodin, 2014), neither GLP1 nor liraglutide crossed the BBB at endothelial cells, either by diffusion or by GLP1R-mediated uptake (Supplementary Fig. 1d), possibly because this receptor is not expressed by endothelial cells (Supplementary Fig. 1eV). To exclude the possibility that the fluorescent moiety modified the physiological route of liraglutide entry into the CNS, we tested the effects of the radioactively labeled compounds $^{125}$I-GLP1 and $^{125}$I-liraglutide. In the BBB model, both had lower permeability coefficients ($P_{app}$) compared to that of sodium fluorescein, but similar to that of FITC-dextran (FD-4), two markers of paracellular transport. Transcytosed levels of the $^{125}$I-GLP1R-agonists (GLP1 or liraglutide) were not modified by the presence of an excess of unlabeled liraglutide or of the GLP1R antagonist,

exendin 9-39, further indicating that blood-borne liraglutide does not cross BBB endothelial cells to reach the brain (Supplementary Fig. 1d).

We next investigated the role of tanycytes in liraglutide transport using primary cultures in a transwell system (Supplementary Fig. 1f I). Similar to the endothelial BBB model (Supplementary Fig. 1b), tanycytes, which replace the BBB at CVOs (Langlet et al., 2013b; Mullier et al., 2010), expressed organized tight-junction complexes *in vitro*, as they do *in vivo* (Fig. 1b). However, in contrast to endothelial cells (Supplementary Fig. 1e), primary cultured tanycytes also expressed GLP1R (Supplementary Fig. 1f IV), as *in vivo* (Supplementary Figure 1g). We compared the uptake of $^{125}$I-liraglutide (0.7 nM) in the presence or absence of unlabeled liraglutide (10 μM) in the two culture models and found that liraglutide accumulation was approximately 4 times higher in tanycytes than in endothelial cells (Fig. 1c). Competition experiments revealed an S-shaped binding curve with an apparent KM of 300 nM (Fig. 1d), suggesting uptake by a single receptor across tanycytes. Subsequently, pulse-chase experiments *in vitro* revealed the rapid uptake of $^{125}$I-liraglutide by tanycytes and the saturation of the process within 15 minutes. Upon removal of the radiolabeled substrate, its intracellular concentration immediately declined, indicating the exocytosis of the drug from tanycytes (Fig. 1e). Since previous *in vitro* studies have shown that liraglutide activates CREB phosphorylation (pCREB) (Athauda and Foltynie, 2016; Que et al., 2019), we used pCREB as a readout for liraglutide-induced cell activation. Immunohistochemical labeling revealed that the intravenous administration of liraglutide markedly induced pCREB at 1 min in tanycytes and neuron-like cells of the ME and ventromedial ARH (vmARH), compared to saline-treated animals (Fig. 1 f-h). pCREB was also induced in rat primary tanycytes treated with liraglutide, an effect that was blunted by co-treatment with the GLP1R antagonist, exendin 9-39 (Supplementary Fig. 2a). Altogether, these observations suggest that liraglutide obtains access to hypothalamic neurons via GLP1R-expressing tanycytes rather than by crossing BBB vessels, but may also bind directly to vmARH neurons residing outside the BBB (Djogo et al., 2016; Schaeffer et al., 2013; Yulyaningsih et al., 2017).

## Transgenic expression of botulinum toxin in tanycytes impedes liraglutide-mediated neuronal activation in the hypothalamus

To determine whether transcytosis across tanycytes mediates the liraglutide-induced activation of hypothalamic neurons, we used a conditional mouse model expressing the botulinum toxin serotype B light chain (BoNT/B), permitting the inducible cell-specific inhibition of SNARE-mediated exocytosis (Slezak et al., 2012). BoNT/B expression in tanycytes was achieved by injecting the recombinant protein TAT-Cre into the third ventricle of *BoNTB-EGFP*$^{\text{loxP-STOP-loxP}}$ mice, as described previously (Langlet et al., 2013a). Cre- and vehicle-injected animals are hereafter referred to as iBot and control mice, respectively (Fig. 2a). The selective expression of the transgene in tanycytes of iBot mice was confirmed by the co-expression of GFP and BoNT/B in FACS-sorted cells from ME/ARH explants (Supplementary Fig. 2b). Furthermore, these cells expressed mRNA for *Darpp-32* (a tanycytic marker) and *Glp1r*, but, in contrast to GFP-negative cells, did not express *Npy* (a neuronal marker) or *Meca32* (an endothelial cell marker) (Supplementary Fig. 2c). *Glp1r* expression was comparable in GFP-positive and GFP-negative cells, i.e., in tanycytes and

in other GLP1-sensitive hypothalamic cells, including neurons (Supplementary Fig. 2d). We next assessed whether intravenously injected liraglutide could stimulate c-Fos expression in the hypothalamus of iBot mice compared to control littermates. c-Fos expression occurs within minutes after cell activation (Manna and Stocco, 2007), allowing us to identify first-order GLP1R-expressing cells. Ten minutes after the intravenous injection of liraglutide in control anesthetized mice, neurons in the anterior hypothalamic nucleus (AHN), paraventricular nucleus (PVH) and lateral hypothalamic (LHA) area were activated (Supplementary Fig. 3a,b,e). AHN and LHA have not previously been identified as targets of liraglutide treatment (Adams et al., 2018; Salinas et al., 2018), although GLP1 binding sites have been documented in these nuclei (Goke et al., 1995). Notably, liraglutide failed to significantly induce c-Fos expression in hypothalamic neurons of iBot mice (Supplementary Fig. 3c-e). One hour after intraperitoneal injection of liraglutide, neurons in the PVH and the LHA, but not in the AHN, were seen to remain activated in control unanesthetized mice (Fig. 2b,c,f), whereas c-Fos expression was unaffected by liraglutide treatment in iBot littermates (Fig. 2d-f). While liraglutide did not significantly upregulate c-Fos expression in the dorsomedial nucleus of the hypothalamus (DMH) or the zona incerta (ZI) in control mice, its expression in these two regions was lower in liraglutide-treated iBot mice when compared to liraglutide-treated control littermates (Fig. 2b-f). Altogether, these results demonstrate that the blockade of vesicular trafficking in tanycytes blunts acute liraglutide-mediated neuronal activation in the tuberal region of the hypothalamus and suggests that circulating liraglutide enters the hypothalamus via transcytosis through tanycytes.

## GLP1R-dependent tanycytic transport is required for the anti-obesity effects of liraglutide

We next explored the anti-obesity actions of liraglutide in control and iBot littermates after a 3-day treatment (Fig. 3a). We first found in controls that liraglutide markedly reduced energy expenditure (Supplementary Fig. 4a)and food intake (Fig. 3b), while promoting body weight loss and fat mass reduction (Fig. 3c,d) in association with increased fatty acid oxidation (Fig. 3e). However, in iBot mice, these effects were abrogated (Fig. 3b-d,f), suggesting that the central metabolic actions of liraglutide require tanycyte-mediated access to the hypothalamic neural substrate (Adams et al., 2018; Cavalcanti-de-AlbuquerQue et al., 2019; He et al., 2019; Secher et al., 2014). To determine whether GLP1R expression in tanycytes (Supplementary Fig. 1g) plays a role in mediating the effects of liraglutide in the hypothalamus, tanycytic GLPIR expression was specifically knocked down by the AAV1/2-mediated expression of a *Glp1r*-silencing shRNA (*Glp1r*$^{\text{TanycyteKD}}$ mice) and green fluorescent protein (GFP) (Supplementary Fig. 4b). RNAscope in situ hybridization studies revealed that GLP1R was abundantly expressed in cells of the ARH, including in vimentin-immunoreactive tanycytic cell bodies lining the wall of the third ventricle and their processes, in mice transduced with a control virus (Fig. 4a), but was selectively blunted in tanycytes of *Glp1r*$^{\text{TanycyteKD}}$ mice (Fig. 4b). Furthermore, FACS experiments demonstrated that the virus-mediated expression of *Glp1r* shRNA markedly and selectively blunted the expression of *Glp1r* transcripts in GFP-positive cells (Fig. 4c), which expressed mRNA for the tanycytic marker *Gpr50* but not proopiomelanocortin (*Pomc*), indicating that GLP1R-expressing POMC neurons of the ARH were spared (Supplementary Fig. 4c). Like iBot mice, *Glp1r*$^{\text{TanycyteKD}}$ mice were resistant to the effects of liraglutide on food intake (Fig. 4d), body weight reduction (Fig. 4e) and fatty acid oxidation (Fig. 4f and 4g). To investigate

whether the tanycyte-specific blunting of GLP1R expression in *Glp1r*$^{\text{TanycyteKD}}$ mice was linked to an alteration of the GLP1R-dependent transport of blood-borne liraglutide into the hypothalamus, microdialysis probes were implanted into the dorsomedial hypothalamus of AAV1/2-transduced mice (Fig. 4h). Thirty minutes after an intraperitoneal bolus of liraglutide, an ELISA for GLP1 (which also recognizes related peptides such as liraglutide) (Supplementary Fig. 4d) revealed a significant peak in the concentration of these peptides in intrahypothalamic dialysates from control mice but not from *Glp1r*$^{\text{TanycyteKD}}$ mice (Fig. 4i). Altogether, these results demonstrate that tanycytic GLP1R binding is required for the transport of blood-borne liraglutide into the hypothalamus, where it exerts its effects on food intake and lipid metabolism.

## Discussion

Several studies to date have shown that the effects of liraglutide on weight loss are predominantly mediated by its actions in the brain (Adams et al., 2018; Beiroa et al., 2014; Fortin et al., 2020; Secher et al., 2014; Sisley et al., 2014). Although the exact route of entry of liraglutide into the brain has not been investigated, previous studies have reported the direct entry of blood-borne GLP1 and its analog, exendin-4, into the brain across the BBB (Kastin and Akerstrom, 2003; Kastin et al., 2002). However, our present results indicate that blood-borne liraglutide does not cross the BBB through endothelial cells, which do not appear to express GLP1R, but by transcytosis through hypothalamic tanycytes, which, in conjunction with the fenestrated vessels of the ME, are also components of the BBB (Prevot et al., 2021). This route of entry is in perfect accord with the key role played by the tanycytic shuttle in transporting other peripheral metabolic signals, such as leptin, ghrelin and insulin, into the mediobasal hypothalamus (Balland et al., 2014; Collden et al., 2015; Duquenne et al., 2021; Porniece Kumar et al., 2021).

The actions of liraglutide in the hypothalamus are extremely rapid – it is internalized by tanycytes in a matter of seconds following its administration, and activates responsive neurons in deeper nuclei that are shielded by the BBB in a matter of minutes. Interestingly, blocking the tanycytic liraglutide shuttle blunts the activation of deeper neurons as well as changes in food intake, fatty acid oxidation and weight loss, indicating the critical importance of the tanycyte-mediated access of liraglutide to hypothalamic nuclei protected by the BBB for its metabolic effects. In fact, even though liraglutide directly activates pCREB in neurons bordering the ME by extravasation from fenestrated vessels, in order to exert its effects on neurons protected by the BBB, such as those of the dorsomedial ARH, its transport across the BBB by tanycytes is essential. This dual mode of access is also similar to that observed with leptin (Duquenne et al., 2021). Moreover, by knocking-down GLP1R specifically in tanycytes, we demonstrate that liraglutide transcytosis into the brain and its anti-obesity effects require tanycytic GLP1R binding and the activation of its downstream signaling cascade, again evoking the receptor-mediated transcytotic mechanism involved in leptin transport (Duquenne et al., 2021). It remains to be seen how tanycytic barrier properties, which are modulated by energy status (Langlet et al., 2013a), and their transport of GLP1R agonists may themselves be altered by obesity (or T2D), thus affecting the entry and efficacy of the very drugs needed to treat it.

Europe PMC Funders Author Manuscripts

To conclude, our study reveals that liraglutide acts directly on its target neurons in the hypothalamus to improve energy homeostasis, and pinpoints the role of tanycytes, which express GLP1R and actively transport blood-borne liraglutide into the brain, in this process. Our results further cement the position of these unique cells, which act as a bridge between the peripheral circulation and the brain, as master regulators of the body's energy/metabolic status.

### Limitations of the study

In order to identify the route of entry of liraglutide by catching it *in flagrante delicto*, in the process of crossing the BBB, and determine the consequences of its action through its immediate target neurons in the hypothalamus, we limited our studies to a 3-day treatment. However, while this was sufficient to identify the tanycytic shuttle as essential for liraglutide transport into the brain, and while a previous study has shown that the effects of liraglutide on food intake are attenuated after the first 24h (Fortin et al., 2020; Killion et al., 2018), it is entirely possible that some of these effects are cumulative (Secher et al., 2014; Sisley et al., 2014) or that the long-term effects of GLP1R agonists on food intake through other brain areas, such as the area postrema or the nucleus of the solitary tract (Brierley et al., 2021; Fortin et al., 2020), contribute to their efficacy. Further evaluation of the effects of liraglutide or other GLP1R agonists at longer time points is necessary to completely understand the mode of action of these drugs on the brain.

## Star Methods

### Resource Availability

**Lead contact—**Additional information and requests for reagents and resources should be directed to and will be fulfilled by the lead contact, Dr. Vincent Prevot (Vincent.prevot@inserm.fr).

**Materials availability—**This study did not generate new unique reagents.

**Data and code availability—**- Data S1. Unprocessed data underlying the display items in the manuscript, related to Figures 1-4, S1-4.

- This paper does not report original code

### Experimental Model And Subject Details

**Animals—**All C57Bl/6J mice and Sprague Dawley rats were housed under specific pathogen-free conditions in a temperature-controlled room (21-22°C) with a 12h light/dark cycle and *ad libitum* access to chow diet (Scientific Diets, SAFE A03) and water. Health status checks of the animal house were performed 4 times *per* year by the animal facility staff to assure the pathogen-free status. *tdTomato*$^{\text{loxP-STOP-loxP}}$, C57BL/6J background, (Stock No.007914; RRID:IMSR_JAX:007914) were purchased from the Jackson Laboratories (Bar Harbor, ME, USA) and Tg(CAG-BoNT/B,EGFP)U75-56wp/J, C57BL/6J background, mice have been engineered by Dr. Franck Pfrieger (University of Strasbourg, France; JAX Stock No. 018056; (RRID:IMSR_JAX:018056) as previously

described (Slezak et al., 2012). Transgenic model mice were bred and genotyped in house to generate experimental animals. Control male C57Bl/6J (RRID:MGI:5657312) mice were purchased from Charles River. Male Sprague Dawley (RRID:MGI:5651135) rats were purchased from Janvier laboratories (France) or Taconic (Denmark). All experiments were performed in 8-10 weeks-old male mice and in P2-P10 rat pups of both sexes and 8 weeks-old male rats. All animals were habituated to handling and experimental conditions prior to experimentation and littermate controls were used.

Animal studies were performed with the approval of the Institutional Ethics Committees for the Care and Use of Experimental Animals of the University of Lille and the French Ministry of National Education, Higher Education and Research (APAFIS#2617-2015110517317420 v5) and under the guidelines defined by the European Union Council Directive of September 22, 2010 (2010/63/EU).

## Primary cultures

**Astrocytes:** Rat primary astrocytes were isolated from the cerebral cortices of 2-4 days old Sprague Dawley rat pups as previously described (Hertz et al., 1989). In brief, the rat pups were decapitated and the pooled cortices were pushed through an 80 μm nylon net filter (Millipore) into Dulbecco's modified Eagle's medium (DMEM) with 20 % fetal bovine serum. The cell suspension was cultured in T75 culture flasks (2 flasks per brain) until confluent. Serum content was gradually reduced to 15 and 10 % through a period of three weeks. During the final week, the cell culture medium was harvested as astrocyte-conditioned medium (ACM). Cells were passaged, frozen at -80 °C and subsequently stored in liquid nitrogen.

**Brain capillaries:** Primary brain capillaries were isolated from the brain cortices of calves below 12 months (Mogens Nielsen Kreaturslagteri A/S), and from rat and mice cerebral cortices using the same techniques of recovering the microvessels form grey matter suspension, but adapted to the size of the different species as previously described (Helms and Brodin, 2014). Capillaries were frozen in aliquots (10 per brain) and stored in liquid nitrogen until their use in culture. In brief, rat brain capillaries were isolated from 8 weeks old male Sprague Dawley rats. Six cortices were isolated using blunt dissection and the meninges were removed by rolling the cortices on filter paper. The cortices were put into DMEM (5 ml per cortex) and homogenized using a 7 ml Dounce Tissue Grinder (Wheaton Science Products). The homogenates were mixed 1:1 with a 32 % (w/v) dextran solution (60000-76000 kDa, Sigma-Aldrich, D8821), and centrifuged (1500 g, 15 minutes). The capillary enriched pellet was washed once in DMEM and filtered through 80 μm nylon net filters (Millipore). The capillaries were digested for 30 minutes with papain dissociation system according to the manufacturer's protocol (Worthington Biochemical). The digested microvessels were seeded directly in culture flasks (one T75 for 6 rat cortices) pre-coated with collagen IV and fibronectin (10 μg/ml of both; Millipore CC076 and FIBRP-RO, respectively).

**Tanycytes:** Primary cultures of tanycytes were generated by isolating the median eminence of 10-day-old Sprague-Dawley rat pups. After median eminence dissociation, cells were

incubated with selective tanycyte medium as previously described (Prevot et al., 2003). In brief, thirty rat pups were decapitated and the median eminences were microdissected and pooled into DMEM + 10 % donor bovine serum. The collected median eminences were pushed through a 20 μm nylon net filter and the resulting cell suspension was seeded in a T75 flask and cultured for 10 days before initial change of culture medium. Medium was then changed every 2-3 days for an additional week of culture. Cells were passaged and seeded on permeable supports 17 days after isolation.

## Method Details

**Stereotaxic TAT-Cre delivery—**Tanycyte-specific genetic modification was performed with the Cre/LoxP system by stereotaxic infusion of a TAT-Cre fusion protein as previously described (Peitz et al., 2002). TAT-cre or vehicle was stereotaxically infused into the third ventricle (2 μl; at 0.2 μl/min; anteroposterior, -1.7 mm; midline, 0 mm; dorsoventral, -5.6 mm) of isoflurane-anesthetized *tdTomato*$^{\text{loxP-STOP-loxP}}$ or *BoNTB-EGFP*$^{\text{loxP-STOP-loxP}}$ mice 2 weeks before commencing the experiments.

**GLP1R knockdown in tanycytes—**Tanycytic specific knockdown of GLP1R was performed in of isoflurane-anesthetized 8-weeks old wild type C57Bl/6J male mice (Charles Rives), by stereotaxically injection of either AAV1/2-shRNA-GLP1R (AAV1/2-EGFP-U6-mGLP1R-shRNA (ACC GCG TCA ACT TTC TTA TCT TC ACT CGA GTG AAG ATA AGA AAG TTG ACG C TTTTT); serotype 1:2 chimeric; titer=5.7 x $10^{10}$; Vector Biolabs) or AAV1/2-GFP (AAV1/2-EGFP-U6(SapI); serotype 1:2 chimeric; titer=6.5 x $10^{10}$; Vector Biolabs) in the lateral ventricle (2 μl; at 0.2 μl/min; anteroposterior, -0.3 mm; midline, -1 mm; dorsoventral, -2.5 mm), 2 weeks before starting the experiments.

***In vivo* Brain Microdialysis—**Male control and GLP1R$^{\text{tanKO}}$ between 30-35g were deeply anesthetized with isoflurane (3% in 1 L/min air flow) in an induction chamber, placed in a stereotaxic apparatus equipped with a mask to maintain anesthesia during all the experiment (isoflurane 1% in 0.7 L/min air flow). Body core temperature was maintained at 37 °C with an electrical blanket controlled by a thermostat. A microdialysis cannula (CMA7, 6 kDa, 2 mm membrane length; CMA microdialysis AB, Sweden) was stereotaxically implanted in the mediobasal hypothalamic area (antero-posterior: -1.4; midline; −0.3 dorsoventral: −6.2 mm). Microdialysis probe was first perfused with sterile artificial cerebrospinal fluid (CMA Perfusion Fluid CNS. NaCl 147 mmol/L, KCl 2.7mmol/L, CaCl2, 1.2 mmol/L and MgCl2 0.85 mmol/L; CMA, Stockholm, Sweden) at a rate of 2 μL/min using a microinjection pump (CMA 402; CMA). Following a stabilization period of 55 min, one dialysate of 15 min was collected to use as a basal reading. At the end of the basal collection, a liraglutide (0.1 mg/Kg) was intraperitoneally administrated and five dialysates every 15 min were recovered. Brain dialysates were placed in a fraction collector (CMA/820) during the experiment and immediately stored at −80°C until analysis. At end of experiment, mice were euthanized by decapitation and brains stored immediately in fresh paraformaldehyde 4%. Brain section of 80 μm were cut in vibratome and counterstained with DAPI (BD Biosystems) to verify proof localization and GFP immunohistochemistry to proof AAV1/2 injection.

**Intrajugular administration of liraglutide—**Under ketamine-xylazine anesthesia (100 mg/Kg, 20 mg/Kg respectively), an intravenous catheter (Optiva® Jelco IV Catheter Radiopaque, 24G, REF5063) was implanted in the exposed right branch of the jugular vein of 8-10 weeks year old male mice. Either fluorescent (liraglutide$^{564}$) or no fluorescent (both provided by Novo Nordisk) were administrated (90 nmol/Kg), and animals were euthanatized at different time points by either decapitation for brain post-fixation for 4 hours in PBS 0.1M -4 % paraformaldehyde (PFA, pH 7.4) after fluorescent liraglutide$^{564}$ injection or transcardially perfused with 20 mL of saline followed by either borate 0.1M-4% PFA buffer (pH 9.5) or 0.1M PBS-4% PFA buffer (pH 7.4) (for c-Fos and pCREB immunohistochemistry respectively) after non-labelled liraglutide injection. Brains were collected, post-fixed in the same fixative for 2 to 4 hours at 4°C, cryoprotected with PB 20% sucrose, and embedded in OCT embedding medium (Tissue-Tek), frozen in isopentane, cooled with dry ice, and stored at -80°C until coronal cryosectioning. Serial coronal sections through the rostro-caudal extent were cut on a cryostat (Leica CM3050S; Leica Microsystems) and either adhered to Superfrost/Plus glass slides (Fisher Scientific Co.) to obtain four sets of slides for post-fixed 18 µm-thick sections after liraglutide$^{564}$ injection, or perfused 30 µm-thick sections were collected free floating in 0.01M PBS for c-Fos and pCREB immunohistochemistry after non-labelled liraglutide administration. The slide-adhered brain sections were desiccated at room temperature for 4 hours and stored at -80 C. Free-floating tissue sections were kept at 4C in anti-freezer solution until processed for double-labeling immunofluorescence.

**Indirect calorimetry study—**Mice were individually housed and acclimatized to the cages for 48h before experimental measurements in a 12h light/dark cycle (lights from 07:00 to 19:00 hours) and an ambient temperature of 22 ± 1°C. Thereafter all mice were injected at 14h saline (200 µl) during 3 consecutive days and then injected with liraglutide (Sisley et al., 2014) (0.1 mg/kg) for 3 consecutive days. Mice were analyzed for total energy expenditure, oxygen consumption and carbon dioxide production, food intake using calorimetric cages (Labmaster, TSE Systems GmbH) (Tschöp et al., 2012). Fat oxidation was calculated as described before (Bruss et al., 2010), using energy expenditure, oxygen consumption and carbon dioxide production. Mice were monitored daily for body weight and body composition at the beginning and the end of the experiment. Body mass composition (lean tissue mass, fat mass, free water and total water content) was analyzed using a body composition scanner by nuclear magnetic resonance (NMR) technology (Minispec mq series, Bruker) according to manufacturer's instructions.

**Isolation of tanycytes by FACS—**The ME from TAT-Cre injected *tdTomato*$^{loxP/+}$ , *BoNTB-EGFP*$^{loxP/+}$ and AAV1/2 GFP control or AAV1/2 GFP-shRNA-GLP1R injected mice were microdissected, and enzymatically dissociated using Papain Dissociation System (Worthington Papain) to obtain single-cell suspensions as described before (Messina et al., 2016). Fluorescence Activated Cell Sorting (FACS) experiments were performed using an EPICS ALTA Cell Sorter Cytometer device (Beckman Coulter). The cell sort decision was based on measurements of tdTomato fluorescence or EGFP fluorescence (Tomato: excitation 488nm, detection: bandpass 675+/-20nm; EGFP: excitation: 488 nm; 50 mW; detection: EGFP bandpass 530/30 nm, autofluorescence bandpass 695/40 nm) by comparing

cell suspensions from non-infected brain sites (the cortex) and infected brain sites (median eminence). For each animal, 4000 cells tdTomato positive or 200 cells EGFP positive and negative cells were sorted directly into 10µL extraction buffer: 0,1% Triton® X-100 (Sigma-Aldrich) and 0,4 U/µl RNaseOUT™ (Thermo Fisher).

**Quantitative RT-PCR analyses—**For gene expression analyses, mRNAs obtained from FACS-sorted tanycytes, were reverse transcribed using SuperScript® III Reverse Transcriptase (Thermo Fisher) and a linear preamplification step was performed for the sorted cells using the TaqMan® PreAmp Master Mix Kit protocol (P/N 4366128, Applied Biosystems). Real-time PCR was carried out on Applied Biosystems 7900HT Fast Real-Time PCR System (RRID:SCR_018060) using exon-boundary-specific TaqMan® Gene Expression Assays: GLP1R (Mm00445292_m1), DARPP32 (Ppp1r1b_Mm00454892_m1), GPR50 (Mm00439147_m1), NPY (NPY-Mm03048253_m1), POMC (Mm00435874_m1) and MECA32 (Plvap-Mm00453379_m1). Control housekeeping genes: r18S (18S-Hs99999901_s1); ACTB (Actb-Mm00607939_s1). Gene expression data were analyzed using SDS 2.4.1 and Data Assist 3.0.1 software (Applied Biosystems).

**Hormone measurements—**Microdialysis samples were analyzed using Northern Lights Mercodia Total GLP-1 NL-ELISA (Mercodia Inc, Cat# 10-1278-01, RRID: AB_2892202) according to the manufacturer's instructions.

### Establishment of *in-vitro* BBB and tanycyte-models

**Bovine endothelial/rat astrocyte BBB vessel model:** Frozen bovine brain capillaries from liquid nitrogen storage were thawed and cultured for 4 days (37 °C, 10 % $CO_2$) in DMEM-Comp (D6429 medium, Sigma-Aldrich): ACM (1:1) supplemented with 125 µg/ml heparin in collagen type IV/fibronectin coated T75 flasks. For the first two days after thawing, the medium was supplemented with 4 µg/ml puromycin to kill pericytes. The endothelial cells were passaged with a brief trypsinization and seeded on collagen IV/fibronectin coated Transwell polycarbonate permeable supports (90 000 cells/$cm^2$, Area = 1.12 cm2, pore radius = 0.4 µm, Corning Life Sciences). Astrocytes were seeded on the bottom of the supports two days prior to endothelial cell seeding (120 000 cells/$cm^2$). The co-cultures were cultured for three days in DMEM-Comp + 125 µg/ml heparin under a humid atmosphere of 5% $CO_2$ and 95% air at 37 °C, followed by three days of culture in differentiation medium consisting of DMEM without NaHCO3- (D5648 medium, Sigma-Aldrich), supplemented with 10 % fetal bovine serum (Gibco), 1 % (v/v) non-essential amino acid mixture, 100 U/ml - 100 µg/ml penicillin-streptomycin solution, 312.5 µM 8-(4-CPT)-cyclic adenosine monophosphate (all Gibco), 0.5 µM dexamethasone (all Merck Millipore), 17.5 µM RO-20-1724 (Calbiochem) and 50 mM 4-(2-Hydroxyethyl)piperazine-1-ethanesulfonic acid (HEPES, all Gibco).

**Endothelial rat/mouse BBB vessel model:** Endothelial cells from rat and mouse brains were cultured for 4-5 days in a culture flask, in mouse endothelial cell culture medium using the supplement kit (PB-M1168-KIT, PeloBiotech), which contained 4 µg/ml puromycin for the two first days. Endothelial cells were passaged similar to the bovine cells and seeded in monocultures on coated permeable supports (90 000 cells/$cm^2$). The endothelial cells

were cultured for two days in mouse endothelial cell culture medium (with supplement kit) followed by three days in differentiation medium as described (Helms and Brodin, 2014), under a humid atmosphere of 5% $CO_2$ and 95% air at 37 °C.

**BBB tanycytes model:** Tanycytes were passaged and seeded in monocultures on coated permeable supports (90 000 cells/$cm^2$) 17 days after isolation similar to the endothelial cells. The tanycytes were then cultured for four days in DMEM (D5796 medium, Sigma-Aldrich) complemented with 10% donor bovine serum, followed by three days in serum-free medium consisting of DMEM/F12 (D6434 medium, Sigma-Aldrich) with 15 mM HEPES, 1% penicillin/streptomycin, 1% L-glutamine (all Gibco), bovine insulin (5 μg/ml) and putrescine (100 μM) (all Sigma-Aldrich), under a humid atmosphere of 5% $CO_2$ and 95% air at 37 °C.

**TEER and transport assessments—**Transcellular transport studies were performed in the BBB models on day 6 on a permeable support. The transendothelial electrical resistance (TEER) was measured at room temperature prior to all experiments, using an Endohm-12 cup electrode chamber (World Precision Instruments) connected to a Millicell-ERS device (Millipore). The culture medium was replaced with pre-heated uptake buffer (as described above) and the cells were added to a solution containing $^{125}$I-GLP-1 (0.5 nM, 1 μCi/ml), $^{125}$I-liraglutide (0.7 nM, 1 μCi/ml), 4 kDa FITC-dextran (10 mg/ml) (Sigma-Aldrich) or sodium fluorescein (1 mg/ml) (Merck Millipore) to the apical compartment. Transport of the radiolabeled compounds was investigated alone and in the presence of 10 μM unlabeled compound or 1000 nM exendin9-39. The cells were placed on a temperature-controlled shaking table at 37 °C for 90 rounds per minute. Samples were taken from the receiver compartment after 30, 60, 120, 180 and 240 minutes and from the donor compartment after 240 minutes (to confirm mass balance). After 240 minutes, the experiments were terminated and permeable supports were washed and collected as described above. Samples were transferred to Ultima Gold scintillation fluid (Perkin-Elmer) and treated as described above.

**Uptake studies—**On day 6 (BBB vessel model) or day 7 (BBB tanycytes model), on permeable-transwell supports, the culture medium was replaced with Hank's balanced salt solution with calcium and magnesium (Gibco) supplemented with 0.1 % ovalbumin (Sigma-Aldrich), 0.005 % Tween 20 and 10 mM HEPES (Gibco) (pH set to 7.4) (uptake buffer). The cells were incubated 15 minutes at 37 °C with in clean uptake buffer or uptake buffer + 1000 nM exendin9-39. For uptake of fluorescently-labelled compounds (Alexa 594-liraglutide or Alexa 488-GLP-1), the cells were added either clean uptake buffer (control) or uptake buffer + fluorescently-labelled compound (final concentration of 100 nM) to the apical compartment and incubated one hour at 37 °C with shaking. For uptake of $^{125}$I-liraglutide, the cells were added to uptake buffer containing 0.7 nM $^{125}$I-liraglutide (1 μCi/ml) with varying amounts of unlabeled liraglutide (10 – 10 000 nM) in the apical compartment and uptake buffer in the basolateral compartment. The cells were incubated 60 minutes at 37 °C with shaking. Receiver and donor samples were withdrawn, the uptake buffer was aspirated and the cells were washed three times in ice-cold uptake buffer. The supports from the uptake studies with fluorescently-labelled compounds were fixed in 4 % paraformaldehyde, permeabilized in 0.1 % triton x-100 and blocked in phosphate buffered saline + 2 % bovine

serum albumin (Sigma-Aldrich). The cells were subsequently incubated with Hoechst (1 μg/ml) and visualized using confocal microscopy as above. The supports from the isotope experiments were either cut out to quantify uptake or added fresh uptake buffer to measure release. For the release studies, the cells were incubated up to one hour in uptake buffer. The permeable supports were put into a picocount scintillation plate (PicoPlate-96, Perkin Elmer) and counted in a (Perkin Elmer). Counts per minute were converted to molar quantities using a standard curve of $^{125}$I-liraglutide in uptake buffer run in parallel. The amounts were standardized relative to the amounts present in the individual donor solutions to obtain the amount of compound taken up relatively to the amount added.

### Immunohistochemistry

**In vitro models:** Freshly isolated mouse capillary fragments, tanycyte- and endothelial cell cultures were fixed in methanol:acetone (1:1) for 1 minute at -20°C, washed three times in PBS + 2 % bovine serum albumin and subsequently blocked for 30 minutes in the same buffer. Samples were incubated with primary antibodies, rabbit claudin-5 (1:200, 34-1600, Zymed, Thermo Fisher; RRID:AB_2533157), rabbit Phospho-CREB (1:400; 9198s, Cell Signaling, Danvers, MA, USA; RRID:AB_2561044), rabbit GFAP (1:2000, Z0334, DakoCytomation, DakoCytomation, Glostrup, Denmark; RRID:AB_10013382), mouse GLP1-R (1:1000, mouse anti-mouse MAB 7f38 Novo-Nordisk; RRID:AB_2618101), chicken vimentin (1:2000, AB5733 Merck Millipore, Burlington, MA, USA; RRID:AB_11212377), rabbit von Willebrand's Factor (1:200, F3520, Sigma-Aldrich; RRID:AB_259543), rabbit PECAM-1 (1:500, sc1506, Santa Cruz Biotechnology, Dallas, TX, USA; RRID:AB_2161037), or mouse ZO-1 (1:200, 339111, Zymed, Thermo Fisher; RRID:AB_87182) in different combinations over night at 4 °C. Following three washing steps of five minutes, samples were incubated with Alexa 488 or Alexa 568-conjugated secondary antibodies, either goat α-rabbit IgG (1:200; Alexa 488, A11008, RRID:AB_143165; Alexa 568 A11011, RRID:AB_143157 Invitrogen, Carlsbad, CA, USA), goat α-mouse IgG (1:200, Alexa 488, A11002, RRID:AB_1500639; Alexa 568, A11031, Invitrogen, RRID:AB_144696) or goat α-chicken IgG (1:200, Alexa 568, A11041, Invitrogen; RRID:AB_2534098) combined with Hoechst 33258 (pentahydrate bis-benzimide, 1μg/mL, Invitrogen, RRID:AB_2651133) for one hour at room temperature.

**In vivo models:** As detailed above, 18 μm post-fixed brain sections from liragluitde$_5$[64] IV-administrated mice were collected in slides, and after 3 washes in 0.01 M PBS, an immunohistochemistry of vimentin (AB5733, Merck Millipore, RID:AB_11212377) was performed as described before (Langlet et al., 2013b), followed by an incubation with Alexa 488-conjugated secondary antibody goat anti-chicken IgG (1:400, A11039, Invitrogen, RRID:AB_142924).

**Double immunohistochemistry pCREB-vimentin:** Ten minutes after saline or liraglutide IV administration (90 nmol/Kg), 30 μm free-floating perfused sections were incubated with both chicken anti vimentin (AB5733, Merck Millipore, RID:AB_11212377) and rabbit anti phospho-CREB (Hagiwara et al., 1993) (provided by Marc R. Montminy, Salk Institute, La Jolla, CA, USA) as previously described (Sanchez et al., 2010).

**c-Fos immunohistochemistry:** One hour or ten minutes after saline or liraglutide IV administration (90 nmol/Kg), control and iBot mice were perfused and brains were processed as described above. A 30 μm free-floating sections were blocked in an incubation solution of PBS, 0.25% bovine serum albumin (BSA, A9418, Sigma-Aldrich), and 0.3% Triton X-100 (T8787, Sigma-Aldrich) with 4% normal goat serum (NGS, D9663, Sigma-Aldrich, RRID:AB_2810235) for 2h at room temperature (RT, 20–25 °C). Then, sections were incubated with rabbit c-Fos antibody (1:500, 226 008, Synaptic Systems, Gottingen, Germany, RRID:AB_2231974) in the same blocking buffer for 48h in agitation at 4 °C. After PBS rinses, sections were incubated with biotinylated-goat anti rabbit antibody (1:400, 111-065-144, Jackson ImmunoResearch, West Grove, PA, USA, RRID:AB_2337965) for 2h at RT. After PBS washes, immunoreactivity was revealed using with Alexa-Fluor 568-streptavidin (1:400, S11226, Invitrogen, RRID:AB_2315774) for 90 minutes. After Hoechst 33258 (pentahydrate bis-benzimide, 1μg/mL, Invitrogen, RRID:AB_2651133) incubation for nuclei visualization, sections were mounted in slides and covered with mount containing Mowiol medium (Calbiochem, Merck Millipore).

**GFP immunohistochemistry:** After the microdialysis experiment in control and $GLP1R^{tanKO}$ mice, brains were collected and postfixed in 4% PFA for 24 hours and then kept in 0.01M PBS-0.05% Na azide until its processing. Brain section of 80 μm were cut in vibratome and free-floating sections were blocked in an incubation solution of PBS, 0.25% bovine serum albumin (BSA, A9418, Sigma-Aldrich), and 0.3% Triton X-100 (T8787, Sigma-Aldrich) with 4% normal goat serum (D9663, Sigma-Aldrich, RRID:AB_2810235) for 2h at room temperature (RT, 20–25 °C). Then, sections were incubated with rabbit GFP antibody (1:500, A11122, Thermo Fisher Scientific Cat# A-11122, RRID:AB_221569) in the same blocking buffer for 48h in agitation at 4 °C. After PBS rinses, immunoreactivity was revealed with Alexa 488-conjugated secondary antibody goat anti-chicken IgG (1:400, A11039, Invitrogen, RRID:AB_142924) for 90 minutes. After Hoechst 33258 (pentahydrate bis-benzimide, 1μg/mL, Invitrogen, RRID:AB_2651133) incubation for nuclei visualization, sections were mounted in slides and covered with mount containing Mowiol medium (Calbiochem, Merck Millipore).

**RNAscope fluorescent *in situ* hybridization—**Mouse GLP1R mRNA fluorescent *in situ* hybridization was performed on frozen brain sections in the mediobasal hypothalamus control and $GLP1R^{tanKO}$ mice with the RNAscope® Multiplex Fluorescent Kit v2 according to the manufacturer's protocol (Advanced Cell Diagnostics, Inc., Newark, CA, USA). Specific probes were used to detect *GLP1R* (Mm-Glp1r-C3, NM_021332.2) mRNA. Hybridization with a probe against the Bacillus subtilis dihydrodipicolinate reductase (dapB) gene (320871) was used as negative control. Following *GLP1R* FISH, a vimentin immunostaining was done using chicken anti-Vimentin antibody (1:500 Millipore Cat# AB1620, RRID:AB_90774), revealed with Goat anti-chicken 647 (1:500; Thermo Fisher Scientific Cat# A-21449, RRID:AB_2535).

**Image Analysis—**The capillaries or cultured endothelial cells were mounted on coverslips and visualized with a Zeiss LSM 510 laser confocal microscope (Carl Zeiss, Jena, Germany, RRID:SCR_018062). Images from brain sections were taken with a Zeiss

20x objective (N.A. 0.8) mounted on an Axio Imager Z2 light microscope (Zeiss, RRID:SCR_018856) or with Zeiss 10x objective mounted on an Axioscan microscope (Zeiss). For FISH experiments and immunofluorescent staining of Vimentin, acquisition of images was performed using an inverted confocal microscope (LSM 710, Zeiss, Jena, Germany) and high magnification photomicrographs were acquired with a 63x objective (NA 1.4) using the Airyscan detector (Zeiss). ImageJ (National Institutes of Health, Bethesda, MD, RRID:SCR_003070) and Photoshop CC (Adobe Systems, San Jose, CA, RRID:SCR_014199) were used to process, quantify, adjust, and merge the photomontages. Image analyses were performed in a blinded manner. Figures were prepared using Adobe Photoshop CC and Adobe Illustrator CC (Adobe Systems, San Jose, CA, RRID:SCR_010279).

### Quantification And Statistical Analyses

No statistical method was used to determine sample size. Data are expressed as means ± s.e.m. To test whether the results followed a Gaussian distribution, a normality test was performed (Kolgomorov– Smirnov test for $n = 5–7$, Shapiro–Wilk test for $n \geq 7$). Results between groups were analyzed using one-way and two-way ANOVA, with Tukey's or Fisher's LSD *post hoc* tests were used for multiple comparisons. Student t-test between control and treatment groups in cases in which statistical significance was established. Differences between two groups were determined using paired or unpaired Mann-Whitney for not Gaussian distributions or one or two-tailed Student's t-tests for Gaussian ones. Statistical analyzes was performed with GraphPad PRISM 8.0 (version 8.4.2; GraphPad Software, La Jolla, California, USA, RRID:SCR_002798). The threshold for significance was $P < 0.05$. All the statistical parameters can be found in the figures and figure legends.

## Supplementary Material

Refer to Web version on PubMed Central for supplementary material.

## Acknowledgements

This work was supported by the European Research Council (ERC) Synergy Grant no. 810331 to VP, H2020-MSCA grant No. 748134 to MI, the Agence National de la Recherche (ANR, France) Grant ANR-15-CE14-0025 to VP, « European Genomic Institute for Diabetes » (E.G.I.D, ANR-10-LABX-0046 and I-SITE ULNE ANR-16-IDEX-0004 to VP, FP and BS), the Conseil Regional Nord-Pas de Calais (to CB), and received funding from Novo Nordisk A/S (SL and VP). HCCH was supported by a fellowship from Novo. BS is a recipient of an ERC Advanced Grant (694717). We thank Marc R. Montminy (Salk Institute, La Jolla, CA, USA) for his generous gift of the phopho-CREB antibody. We thank Emilie Caron (metabolic cages), Nathalie Jouy and Amandine Legrand (cell sorting), Antonino Bongiovani (imaging facility) from the BioImaging Center of Lille (BiCeL), and Julien Devassine (animal core facility) of the PLBS UAR2014-US41 for their expert technical support.

## Data Availability

All unprocessed data that were used to create graphs in Figures 1-4, S1-4 are reported in the spreadsheet Data S1

Europe PMC Funders Author Manuscripts

## References


Adams JM, Pei H, Sandoval DA, Seeley RJ, Chang RB, Liberles SD, Olson DP. Liraglutide Modulates Appetite and Body Weight Through Glucagon-Like Peptide 1 Receptor-Expressing Glutamatergic Neurons. Diabetes. 2018; 67: 1538–1548. [PubMed: 29776968]

Athauda D, Foltynie T. The glucagon-like peptide 1 (GLP) receptor as a therapeutic target in Parkinson's disease: mechanisms of action. Drug Discovery Today. 2016; 21: 802–818. [PubMed: 26851597]

Balland E, Dam J, Langlet F, Caron E, Steculorum S, Messina A, Rasika S, Falluel-Morel A, Anouar Y, Dehouck B, et al. Hypothalamic tanycytes are an ERK-gated conduit for leptin into the brain. Cell Metab. 2014; 19: 293–301. [PubMed: 24506870]

Banks WA. The blood-brain barrier as an endocrine tissue. Nature reviews Endocrinology. 2019; 15: 444–455.

Beiroa D, Imbernon M, Gallego R, Senra A, Herranz D, Villarroya F, Serrano M, Fernø J, Salvador J, Escalada J, et al. GLP-1 agonism stimulates brown adipose tissue thermogenesis and browning through hypothalamic AMPK. Diabetes. 2014; 63: 3346–3358. [PubMed: 24917578]

Brierley DI, Holt MK, Singh A, de Araujo A, McDougle M, Vergara M, Afaghani MH, Lee SJ, Scott K, Maske C, et al. Central and peripheral GLP-1 systems independently suppress eating. Nature metabolism. 2021; 3: 258–273.

Bruss MD, Khambatta CF, Ruby MA, Aggarwal I, Hellerstein MK. Calorie restriction increases fatty acid synthesis and whole body fat oxidation rates. American journal of physiology. Endocrinology and metabolism. 2010; 298 E108-116 [PubMed: 19887594]

Cavalcanti-de-Albuquerque JP, Bober J, Zimmer MR, Dietrich MO. Regulation of substrate utilization and adiposity by Agrp neurons. Nat Commun. 2019; 10

Chambers AP, Sorrell JE, Haller A, Roelofs K, Hutch CR, Kim KS, Gutierrez-Aguilar R, Li B, Drucker DJ, D'Alessio DA, et al. The Role of Pancreatic Preproglucagon in Glucose Homeostasis in Mice. Cell Metab. 2017; 25: 927–934. e923 [PubMed: 28325479]

Collden G, Balland E, Parkash J, Caron E, Langlet F, Prevot V, Bouret SG. Neonatal overnutrition causes early alterations in the central response to peripheral ghrelin. Mol Metab. 2015; 4: 15–24. [PubMed: 25685686]

Djogo T, Robins SC, Schneider S, Kryzskaya D, Liu X, Mingay A, Gillon CJ, Kim JH, Storch KF, Boehm U, et al. Adult NG2-Glia Are Required for Median Eminence-Mediated Leptin Sensing and Body Weight Control. Cell Metab. 2016; 23: 797–810. [PubMed: 27166944]

Drucker DJ, Habener JF, Holst JJ. Discovery, characterization, and clinical development of the glucagon-like peptides. The Journal of Clinical Investigation. 2017; 127: 4217–4227. [PubMed: 29202475]

Duquenne M, Folgueira C, Bourouh C, Millet M, Silva A, Clasadonte J, Imbernon M, Fernandois D, Martinez-Corral I, Kusumakshi S, et al. Leptin brain entry via a tanycytic LepR-EGFR shuttle controls lipid metabolism and pancreas function. Nat Metab. 2021; 3: 1071–1090. [PubMed: 34341568]

Fortin SM, Lipsky RK, Lhamo R, Chen J, Kim E, Borner T, Schmidt HD, Hayes MR. GABA neurons in the nucleus tractus solitarius express GLP-1 receptors and mediate anorectic effects of liraglutide in rats. Sci Transl Med. 2020; 12

Garber AJ. Long-acting glucagon-like peptide 1 receptor agonists: a review of their efficacy and tolerability. Diabetes Care. 2011; 34 (Suppl) 2 S279-284 [PubMed: 21525469]

Garcia-Caceres C, Balland E, Prevot V, Luquet S, Woods SC, Koch M, Horvath TL, Yi CX, Chowen JA, Verkhratsky A, et al. Role of astrocytes, microglia, and tanycytes in brain control of systemic metabolism. Nat Neurosci. 2019; 22: 7–14. [PubMed: 30531847]

Goke R, Larsen PJ, Mikkelsen JD, Sheikh SP. Distribution of GLP-1 binding sites in the rat brain: evidence that exendin-4 is a ligand of brain GLP-1 binding sites. Eur J Neurosci. 1995; 7: 2294–2300. [PubMed: 8563978]

Hagiwara M, Brindle P, Harootunian A, Armstrong R, Rivier J, Vale W, Tsien R, Montminy MR. Coupling of hormonal stimulation and transcription via the cyclic AMP-responsive factor CREB is

rate limited by nuclear entry of protein kinase A. Mol Cell Biol. 1993; 13: 4852–4859. [PubMed: 8336722]

He Z, Gao Y, Lieu L, Afrin S, Cao J, Michael NJ, Dong Y, Sun J, Guo H, Williams KW. Direct and indirect effects of liraglutide on hypothalamic POMC and NPY/AgRP neurons - Implications for energy balance and glucose control. Mol Metab. 2019; 28: 120–134. [PubMed: 31446151]

Helms HC, Brodin B. Generation of primary cultures of bovine brain endothelial cells and setup of cocultures with rat astrocytes. Methods in molecular biology. 2014; 1135: 365–382. [PubMed: 24510879]

Hertz, L, Juurlink, BHJ, Hertz, E, Fosmark, H. A Dissection and Tissue Culture. Manual of the Nervous System. Shahar, A, Vellis, JVAD, Haber, B, editors. Alan R. Liss, Inc; New York: 1989. 105–108.

Holt MK, Richards JE, Cook DR, Brierley DI, Williams DL, Reimann F, Gribble FM, Trapp S. Preproglucagon Neurons in the Nucleus of the Solitary Tract Are the Main Source of Brain GLP-1, Mediate Stress-Induced Hypophagia, and Limit Unusually Large Intakes of Food. Diabetes. 2019; 68: 21–33. [PubMed: 30279161]

Kastin AJ, Akerstrom V. Entry of exendin-4 into brain is rapid but may be limited at high doses. Int J Obes Relat Metab Disord. 2003; 27: 313–318. [PubMed: 12629557]

Kastin AJ, Akerstrom V, Pan W. Interactions of glucagon-like peptide-1 (GLP-1) with the blood-brain barrier. Journal of molecular neuroscience : MN. 2002; 18: 7–14. [PubMed: 11931352]

Killion EA, Wang J, Yie J, Shi SD, Bates D, Min X, Komorowski R, Hager T, Deng L, Atangan L, et al. Anti-obesity effects of GIPR antagonists alone and in combination with GLP-1R agonists in preclinical models. Sci Transl Med. 2018; 10

Kim W, Egan JM. The role of incretins in glucose homeostasis and diabetes treatment. Pharmacol Rev. 2008; 60: 470–512. [PubMed: 19074620]

Kjems LL, Holst JJ, Volund A, Madsbad S. The influence of GLP-1 on glucose-stimulated insulin secretion: effects on beta-cell sensitivity in type 2 and nondiabetic subjects. Diabetes. 2003; 52: 380–386. [PubMed: 12540611]

Langlet F, Levin BE, Luquet S, Mazzone M, Messina A, Dunn-Meynell A, Balland E, Lacombe A, Mazur D, Carmeliet P, et al. Tanycytic VEGF-A boosts blood-hypothalamus barrier plasticity and access of metabolic signals to the arcuate nucleus in response to fasting. Cell Metabolism. 2013a; 17: 607–617. [PubMed: 23562080]

Langlet F, Mullier A, Bouret SG, Prevot V, Dehouck B. Tanycyte-Like Cells Form a Blood–Cerebrospinal Fluid Barrier in the Circumventricular Organs of the Mouse Brain. The Journal of comparative neurology. 2013b; 521: 3389–3405. [PubMed: 23649873]

Manna PR, Stocco DM. Crosstalk of CREB and Fos/Jun on a single cis-element: transcriptional repression of the steroidogenic acute regulatory protein gene. J Mol Endocrinol. 2007; 39: 261–277. [PubMed: 17909266]

Messina A, Langlet F, Chachlaki K, Roa J, Rasika S, Jouy N, Gallet S, Gaytan F, Parkash J, Tena-Sempere M, et al. A microRNA switch regulates the rise in hypothalamic GnRH production before puberty. Nature Neuroscience. 2016. 1–12.

Mullier A, Bouret SG, Prevot V, Dehouck B. Differential distribution of tight junction proteins suggests a role for tanycytes in blood-hypothalamus barrier regulation in the adult mouse brain. J Comp Neurol. 2010; 518: 943–962. [PubMed: 20127760]

Peitz M, Pfannkuche K, Rajewsky K, Edenhofer F. Ability of the hydrophobic FGF and basic TAT peptides to promote cellular uptake of recombinant Cre recombinase: a tool for efficient genetic engineering of mammalian genomes. Proceedings of the National Academy of Sciences of the United States of America. 2002; 99: 4489–4494. [PubMed: 11904364]

Peyot ML, Gray JP, Lamontagne J, Smith PJ, Holz GG, Madiraju SR, Prentki M, Heart E. Glucagon-like peptide-1 induced signaling and insulin secretion do not drive fuel and energy metabolism in primary rodent pancreatic beta-cells. PloS one. 2009; 4 e6221 [PubMed: 19593440]

Porniece Kumar M, Cremer AL, Klemm P, Steuernagel L, Sundaram S, Jais A, Hausen AC, Tao J, Secher A, Pedersen TA, et al. Insulin signalling in tanycytes gates hypothalamic insulin uptake and regulation of AgRP neuron activity. Nat Metab. 2021; 3: 1662–1679. [PubMed: 34931084]

Prevot V, Cornea A, Mungenast A, Smiley G, Ojeda SR. Activation of erbB-1 signaling in tanycytes of the median eminence stimulates transforming growth factor beta1 release via prostaglandin E2 production and induces cell plasticity. J Neurosci. 2003; 23: 10622–10632. [PubMed: 14627647]

Prevot V, Dehouck B, Sharif A, Ciofi P, Giacobini P, Clasadonte J. The Versatile Tanycyte: A Hypothalamic Integrator of Reproduction and Energy Metabolism. Endocr Rev. 2018; 39: 333–368. [PubMed: 29351662]

Prevot V, Nogueiras R, Schwaninger M. Tanycytes in the infundibular nucleus and median eminence and their role in the blood-brain barrier. Handb Clin Neurol. 2021; 180: 253–273. [PubMed: 34225934]

Que Q, Guo X, Zhan L, Chen S, Zhang Z, Ni X, Ye B, Wan S. The GLP-1 agonist, liraglutide, ameliorates inflammation through the activation of the PKA/CREB pathway in a rat model of knee osteoarthritis. Journal of Inflammation. 2019; 16: 13. [PubMed: 31182934]

Salinas CBG, Lu TT, Gabery S, Marstal K, Alanentalo T, Mercer AJ, Cornea A, Conradsen K, Hecksher-Sorensen J, Dahl AB, et al. Integrated Brain Atlas for Unbiased Mapping of Nervous System Effects Following Liraglutide Treatment. Sci Rep. 2018; 8 10310 [PubMed: 29985439]

Sanchez E, Singru PS, Wittmann G, Nouriel SS, Barrett P, Fekete C, Lechan RM. Contribution of TNF-alpha and nuclear factor-kappaB signaling to type 2 iodothyronine deiodinase activation in the mediobasal hypothalamus after lipopolysaccharide administration. Endocrinology. 2010; 151: 3827–3835. [PubMed: 20501675]

Schaeffer M, Langlet F, Lafont C, Molino F, Hodson DJ, Roux T, Lamarque L, Verdie P, Bourrier E, Dehouck B, et al. Rapid sensing of circulating ghrelin by hypothalamic appetite-modifying neurons. Proceedings of the National Academy of Sciences of the United States of America. 2013; 110: 1512–1517. [PubMed: 23297228]

Secher A, Jelsing J, Baquero AF, Hecksher-Sørensen J, Cowley MA, Dalbøge LS, Hansen G, Grove KL, Pyke C, Raun K, et al. The arcuate nucleus mediates GLP-1 receptor agonist liraglutide-dependent weight loss. Journal of Clinical Investigation. 2014; 124: 4473–4488. [PubMed: 25202980]

Sisley S, Gutierrez-Aguilar R, Scott M, D'Alessio DA, Sandoval DA, Seeley RJ. Neuronal GLP1R mediates liraglutide's anorectic but not glucose-lowering effect. J Clin Invest. 2014; 124: 2456–2463. [PubMed: 24762441]

Slezak M, Grosche A, Niemiec A, Tanimoto N, Pannicke T, Munch TA, Crocker B, Isope P, Hartig W, Beck SC, et al. Relevance of exocytotic glutamate release from retinal glia. Neuron. 2012; 74: 504–516. [PubMed: 22578502]

Timper K, Del Rio-Martin A, Cremer AL, Bremser S, Alber J, Giavalisco P, Varela L, Heilinger C, Nolte H, Trifunovic A, et al. GLP-1 Receptor Signaling in Astrocytes Regulates Fatty Acid Oxidation, Mitochondrial Integrity, and Function. Cell Metab. 2020.

Tschöp MH, Speakman JR, Arch JRS, Auwerx J, Brüning JC, Chan L, Eckel RH, Farese RV, Galgani JE, Hambly C, et al. A guide to analysis of mouse energy metabolism. Nature methods. 2012; 9: 57–63.

Yulyaningsih E, Rudenko IA, Valdearcos M, Dahlen E, Vagena E, Chan A, Alvarez-Buylla A, Vaisse C, Koliwad SK, Xu AW. Acute Lesioning and Rapid Repair of Hypothalamic Neurons outside the Blood-Brain Barrier. Cell reports. 2017; 19: 2257–2271. [PubMed: 28614713]

Europe PMC Funders Author Manuscripts

Europe PMC Funders Author Manuscripts

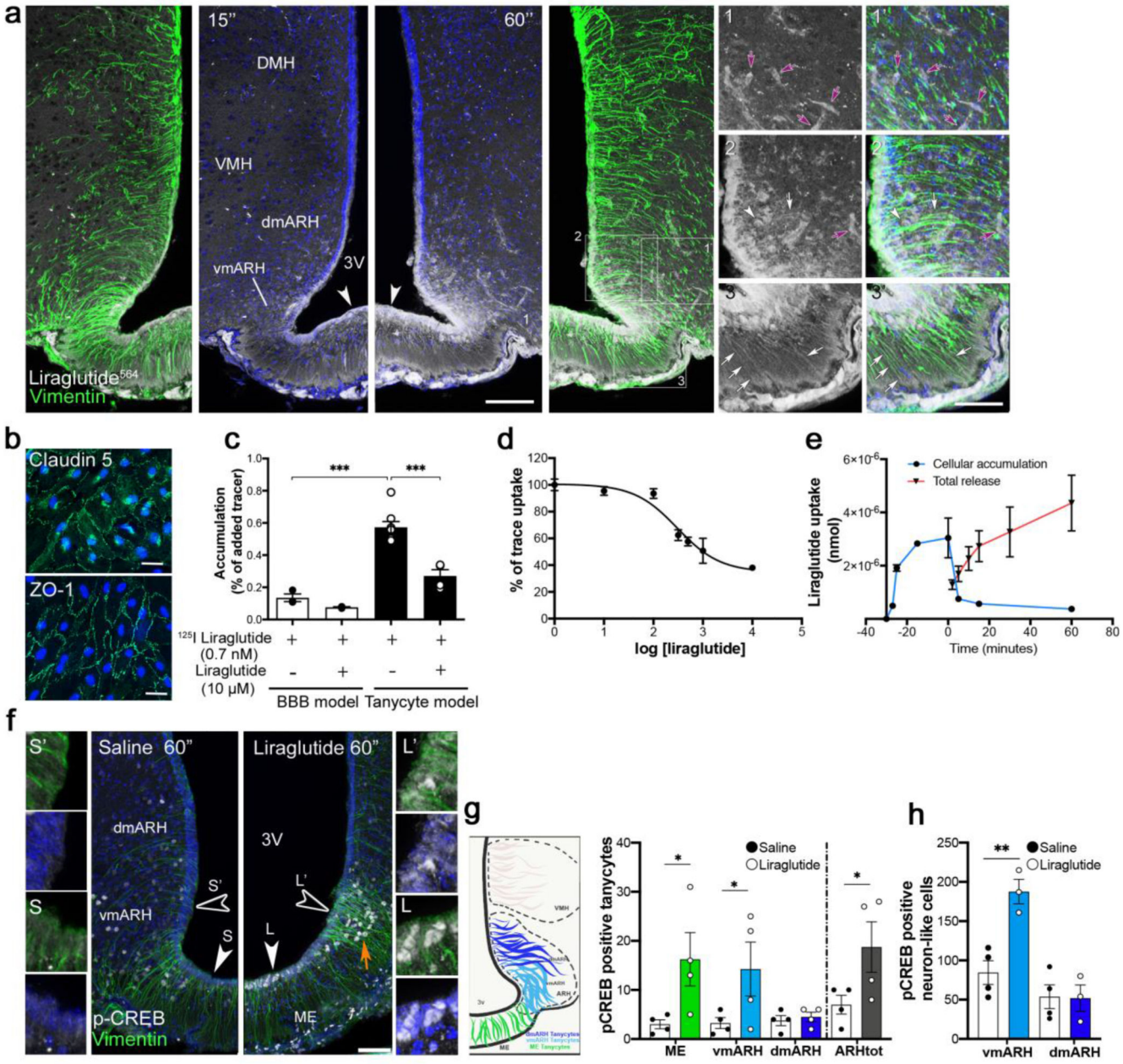


**Figure 1. Blood-borne liraglutide does not cross the brain-blood barrier (BBB) at endothelial cells, but is transcytosed by tanycytes and has direct access to putative neurons lying outside the BBB in the ME.**

(**a**) Representative photomicrographs of the tuberal region of the hypothalamus showing tanycytic processes (arrows) and cell bodies (arrowheads) labelled by vimentin (green) and fluorescent liraglutide$^{564}$ (white), 15 and 60 seconds after intravenous injection (90 nmol/Kg). Note that some neuron-like cell bodies also appear to internalize liraglutide$^{564}$ (red arrowheads) and that liraglutide$^{564}$ does not extravasate from BBB vessels (yellow arrows). Scale bar 200 µm. (**b**) Representative images of immunohistochemical staining for the tight junction markers Claudin-5 (green) and ZO-1 in primary tanycytes. Scale

bar 30 μm. (**c**) Accumulation of $^{125}$I liraglutide with or without unlabeled liraglutide, in endothelial cells of the traditional BBB model (white bars) and in tanycytes (black bars). Data were analyzed using one-way ANOVA ($F_{(6, 19)} = 8.85$; $p = 0.0001$) followed by Tukey's multiple comparison test ($^{125}$I-liraglutide BBB vs. tanycytic model, $p < 0.0001$; $^{125}$I-liraglutide BBB without liraglutide vs. with liraglutide; $p < 0.0001$) ($n = 3, 3, 8, 8$ wells from 2 independent experiments). (**d**) Competition curve of $^{125}$I-liraglutide and increasing concentrations (in nM) of unlabeled liraglutide ($n = 6, 3, 3, 3, 4, 4, 3$ wells from 2 independent experiments). (**e**) Time-dependent accumulation (blue line) and release (red line) of $^{125}$I-liraglutide (cellular accumulation $n = 4, 3, 3, 3, 6, 3,3$ wells from 2 independent experiments; total release $n = 3$). (**f**) Representative photomicrographs showing pCREB in tanycytes and neuron-like cells in the vmARH of mice after treatment with saline (left panel) vs. liraglutide (right panel). Scale bar 150 μm (insets, 50 μm). (**g, h**) Quantification of pCREB-positive tanycytes (g) and neuron-like cells (h) in the ME, vmARH, dmARH and ARHtot. ($n = 4$ animals per group; 3 to 4 sections per animal). (g) Data were analyzed using an unpaired t-test (ME saline vs. liraglutide $t(6) = 2.40$, $p$=0.0265; vmARH saline vs. liraglutide $t_{(6)} = 1.96$, $p = 0.0491$; ARHtot (vmARH + dmARH) saline vs. liraglutide $t_{(6)} = 2.15$, $p = 0.0376$). (h) Data were analyzed using an unpaired one-tailed t-test (vmARH saline vs. liraglutide $t_{(5)} = 4.66$, $p = 0.0028$). ME, median eminence; ARH, arcuate nucleus of the hypothalamus; vm, ventromedial; dm, dorsomedial; tot, total; VMH, ventromedial nucleus of the hypothalamus; DMH, dorsomedial nucleus; 3V, third ventricle. Data are represented as means ± SEM. *$p < 0.05$, ** $p < 0.01$, *** $p < 0.001$.




Europe PMC Funders Author Manuscripts

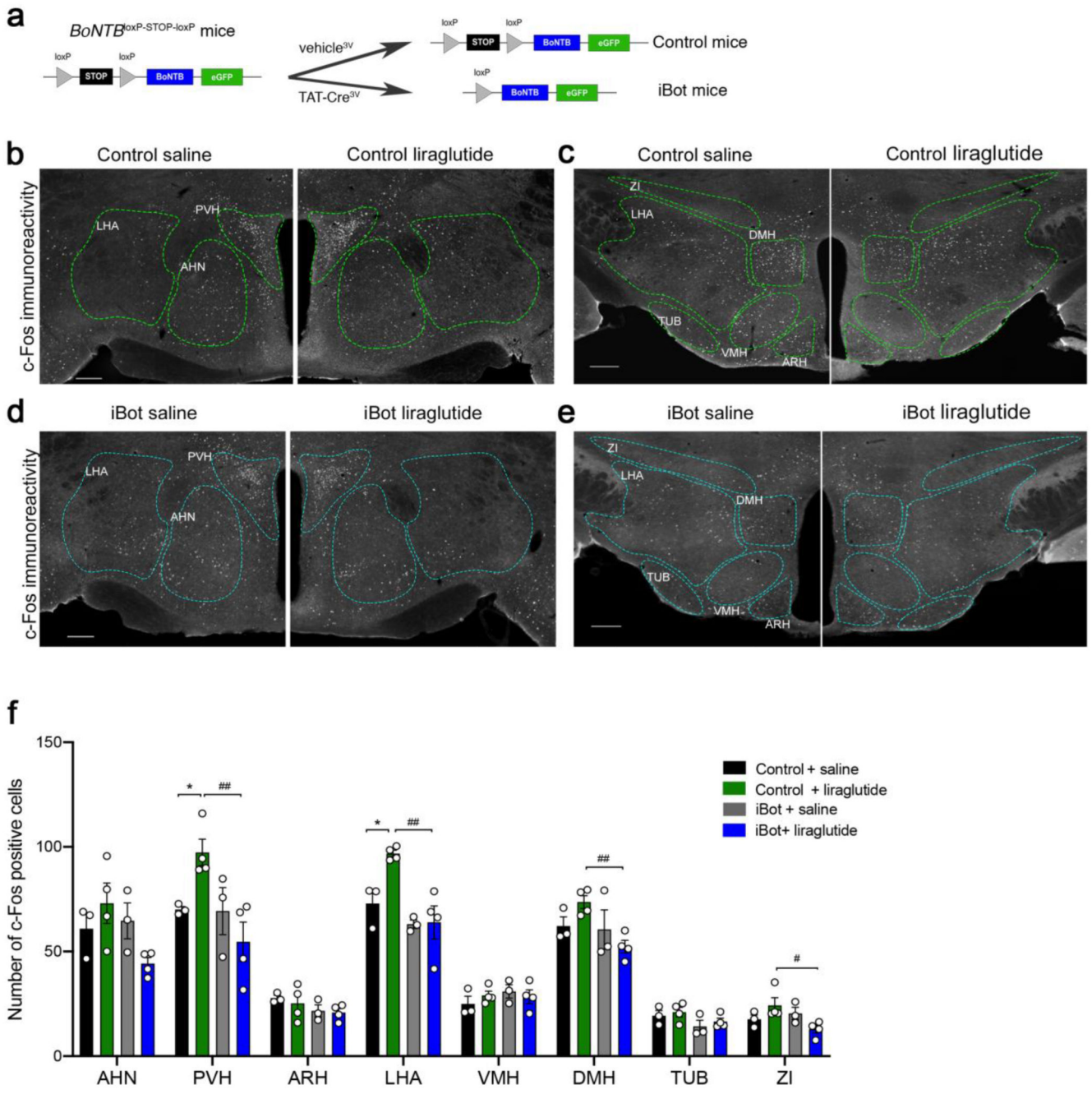


**Figure 2. Liraglutide-induced c-Fos activation is abolished in the hypothalamus of iBot mice selectively expressing botulinum toxin in tanycytes.**

(**a**) Protocol for Cre-dependent induction of *BoNT/B* in tanycytes followed by the injection of recombinant TAT-Cre or vehicle into the third ventricle of *BoNTB-EGFP*$^{loxP\text{-}STOP\text{-}loxP}$ mice. (**b-e**) Representative photomicrographs of c-Fos immunohistochemistry in the hypothalamus of control (**b, c**) and iBot (**d, e**) mice 1h after intraperitoneal injection of saline (left panels) or liraglutide (90 nmol/Kg, right panels). AHN: anterior hypothalamic nucleus; ARH: arcuate nucleus of the hypothalamus; DMH: dorsomedial hypothalamic nucleus; LHA: lateral hypothalamic nucleus; PVH: paraventricular nucleus of the




Europe PMC Funders Author Manuscripts

hypothalamus; TUB: tuberal nucleus; ZI: zona incerta. Scale bar 200 μm. (**f**) Quantification of the number of c-Fos positive cells in mouse hypothalamic sections 1 hour after intraperitoneal injection of either saline (black, grey) or liraglutide (0,1 mg/kg) (green, blue) in control (black and green) and iBot mice (grey and blue). ($n$ = 3, 4, 3, 4 animals per group; 6 to 7 sections per animal). PVH: two-way ANOVA, genotype: $F_{(1, 10)}$= 6.96, $p$ = 0.024; treatment: $F_{(1, 10)}$= 0.586, $p$ = 0.024; interaction: $F_{(1, 10)}$= 6.502, $p$ = 0.0289. Fisher's LSD *post hoc* test, control saline vs. control liraglutide, $p$ = 0.0410 and control liraglutide vs. iBot liraglutide, $p$ = 0.0027. LHA: two-way ANOVA, genotype: $F_{(1, 10)}$= 15.54, $p$ = 0.0028; treatment: $F_{(1, 10)}$= 5.19, $p$ = 0.045; interaction: $F_{(1, 10)}$= 4.468, $p$ = 0.0607. Fisher's LSD *post hoc* test, control saline vs. control liraglutide, $p$ = 0.011 and control liraglutide vs. iBot liraglutide, $p$ = 0.0009. DMH: two-way ANOVA, genotype: $F_{(1, 10)}$= 5.21, $p$ = 0.0456; treatment: $F_{(1, 10)}$= 0.1, $p$ = 0.756; interaction: $F_{(1, 10)}$= 3.827, $p$ = 0.078. Fisher's LSD *post hoc* test, control liraglutide vs. iBot liraglutide, $p$ = 0.0089. ZI: two-way ANOVA, genotype: $F_{(1, 10)}$= 2.25, $p$ = 0.164; treatment: $F_{(1, 10)}$= 0.03, $p$ = 0.871; interaction: $F_{(1, 10)}$= 6.15, $p$ = 0.032. Fisher's LSD *post hoc* test, control liraglutide vs. iBot liraglutide, $p$ = 0.0124. Data are expressed as means ± SEM. *$p$ < 0.05; ** $p$ < 0.01, control saline vs. control liraglutide; # $p$ < 0.05; ## $p$ < 0.01, control liraglutide vs. iBot liraglutide.

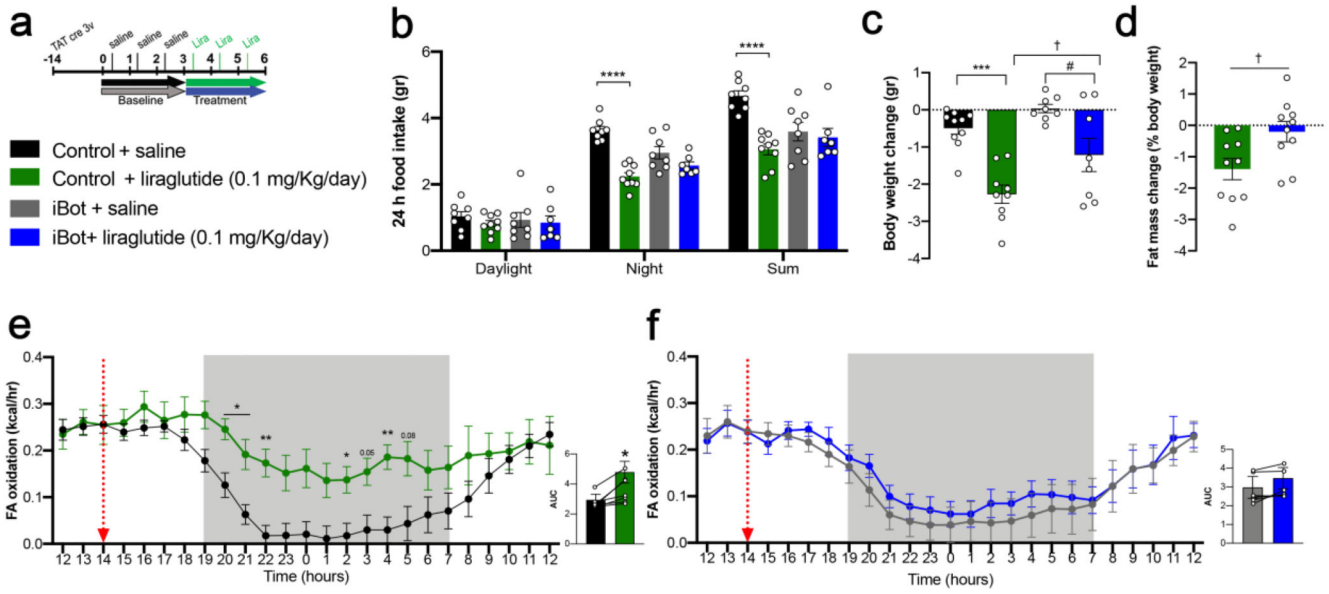


**Figure 3. The anti-obesity effects of liraglutide are abolished by using Botulinum toxin expression to block vesicular transport in tanycytes.**

(**a**) Experimental setup to measure the metabolic effects of liraglutide (panels **b**-**f**). (**b**) Cumulative food intake in the different light/dark phases 3 days after liraglutide treatment, compared to baseline (Night phase: two-way ANOVA, genotype: $F_{(1, 28)}$= 1.64, $p$ = 0.210; treatment: $F_{(1, 28)}$= 42.36, $p$ < 0.0001 interaction: $F_{(1, 28)}$= 13.69, $p$ = 0.0009. Tukey's *post hoc* test, control saline vs. control liraglutide, $p$ <0.0001and iBot saline vs. iBot liraglutide, $p$ = 0.240; sum: two-way ANOVA, genotype: $F_{(1, 28)}$= 2.63, $p$ = 0.116; treatment: $F_{(1, 28)}$= 16.59, $p$ = 0.0003 interaction: $F_{(1, 28)}$= 10.69, $p$ = 0.0029. Tukey's *post hoc* test, control saline vs. control liraglutide, $p$ <0.0001and iBot saline vs. iBot liraglutide, $p$ = 0.945) ($n$ = 8, 9, 8, 7 mice). (**c**) Body weight change after the experiment shown in (**a**) (two-way ANOVA, genotype: $F_{(1, 31)}$= 8.98, $p$ = 0.53; treatment: $F_{(1, 31)}$= 32.85 , $p$ < 0.0001; interaction: $F_{(1, 31)}$= 1.01, $p$ = 0.324. Tukey's post hoc test, control saline vs. control liraglutide, $p$ = 0.0001and iBot saline vs. iBot liraglutide, $p$ = 0.0154; control liraglutide vs. iBot liraglutide, $p$ = 0.042) ($n$ = 10, 9, 8, 8 mice). (**d**) Fat mass change after the experiment shown in (**a**). Data were analyzed using an unpaired one-tailed t-test (fat mass, $t_{(18)}$ = 2.53, $p$ = 0.0104; body weight change, $p$ = 0.0495) ($n$ = 10, 10 mice). (**e, f**) Fatty acid oxidation and area under the curve (AUC) in control (**e**) and iBot (**f**) animals 3 days after liraglutide injection, compared to saline ($n$ = 8 mice per group). Two-way ANOVA with Tukey's *post hoc* test (control saline vs. control liraglutide: 20.00, $p$ = 0.0191; 21.00, $p$ = 0.0311; 22.00, $p$ = 0.0061; 2.00, $p$ = 0.0408; 4.00, $p$ = 0.0066) ($n$ = 9, 8 mice). Red dotted lines indicate liraglutide or vehicle administration. AUC, paired two-tailed t-test $t_{(5)}$ = 3.62 $p$ = 0.0152, $n$ = 6 mice in (**e**) and $t_{(5)}$ = 2.39, $p$ = 0.0624, $n$ = 6 mice in (**f**). iBot saline vs. iBot liraglutide, # $p$ < 0.05; † $p$ < 0.05 control liraglutide vs. *iBot* liraglutide, * $p$ < 0.05, ** $p$ < 0.01, *** $p$ < 0.001, **** $p$ < 0.0001.




Europe PMC Funders Author Manuscripts

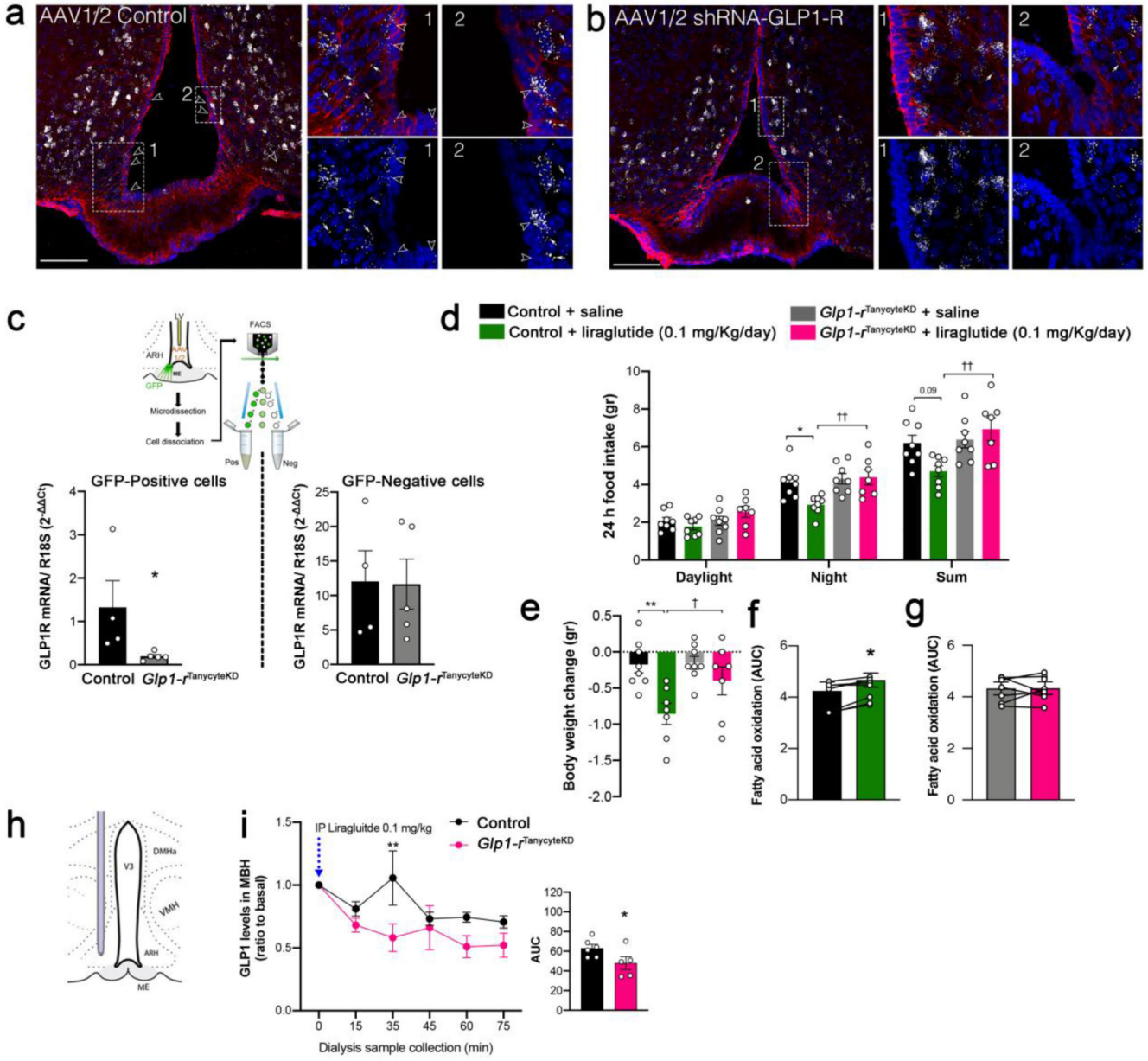


**Figure 4. Knocking down GLP1R in tanycytes abolishes both the shuttling of blood-borne liraglutide into the hypothalamus and its anti-obesity effects.**

(**a**, **b**) Representative photomicrographs of the tuberal region of the hypothalamus showing vimentin-immunoreactive tanycytic processes and cell bodies (red) and GLP1R mRNA expression (white dots) after transduction of tanycytes with a control AAV1/2 (**a**) or an AAV1/2 expressing GLP1R shRNA (**b**). Empty arrowheads indicate tanycytic cell bodies expressing GLP1R in the vmARH and white arrows point to tanycytic processes where vimentin and *Glp1-r* transcripts are colocalized. Scale bar: 200 μm. (**c**) Schematic diagram: sorting of GFP-positive putative tanycytes following AAV1/2 control or AAV1/2 shRNA-GLP1R infusion into the lateral ventricle. Bar graph: expression of GLP1R mRNA in GFP-positive and -negative FACS-sorted cells. Unpaired one-tailed t-test (positive cells;




Europe PMC Funders Author Manuscripts

Europe PMC Funders Author Manuscripts

control vs. GLP1R$^{tanycteKD}$, $t_{(7)}$ = 2.08, $p$ = 0.0377, $n$ = 4, 5 mice). (**d**) Cumulative food intake during the different light/dark phases 3 days after liraglutide treatment, compared to baseline (Night: two-way ANOVA, genotype: $F_{(1, 27)}$= 7.88, $p$ = 0.009; treatment: $F_{(1, 27)}$ = 3.59, $p$ = 0.069; interaction: $F_{(1, 27)}$= 4.72, $p$ = 0.039. Tukey's post hoc test, control saline vs. control liraglutide, $p$ = 0.033 and *Glp1-r*$^{TanycyteKD}$ saline vs. *Glp1-r*$^{TanycyteKD}$ liraglutide, $p$ = 0.99; control liraglutide vs. *Glp1-r*$^{TanycyteKD}$ liraglutide, $p$ = 0.042. Sum: two-way ANOVA, genotype: $F_{(1, 27)}$= 7.64, $p$ = 0.010; treatment: $F_{(1, 27)}$= 1.12 , $p$ = 0.299; interaction: $F_{(1, 27)}$= 5.48, $p$ = 0.027. Tukey's post hoc test, control saline vs. control liraglutide, $p$ = 0.09 and *Glp1-r*$^{TanycyteKD}$ saline vs. *Glp1-r*$^{TanycyteKD}$ liraglutide, $p$ = 0.809; control liraglutide vs. *Glp1-r*$^{TanycyteKD}$ liraglutide, $p$ = 0.007; $n$ = 8, 8, 8, 7 mice). (**e**) Body weight change after the experiment (two-way ANOVA, genotype: $F_{(1, 26)}$= 3.07, $p$ = 0.091; treatment: $F_{(1, 26)}$= 11.48 , $p$ = 0.0022 interaction: $F_{(1, 26)}$= 2.47, $p$ = 0.128. Tukey's post hoc test, control saline vs. control liraglutide, $p$ = 0.0017and *Glp1-r*$^{TanycyteKD}$ saline vs. *Glp1-r*$^{TanycyteKD}$ liraglutide, $p$ = 0.210; control liraglutide vs. *Glp1-r*$^{TanycyteKD}$ liraglutide, $p$ = 0.031, $n$ = 8, 7, 8, 7 mice). (**f, g**) AUC of 24h fatty acid oxidation in control (**f**) and *Glp1r*$^{tanycyteKD}$ (**g**) animals 3 days after liraglutide injection, compared to saline ($n$ = 8 mice per group). Paired two-tailed t-test $t_{(6)}$ = 3.62, p=0.011 in **f** ($n$ = 7 mice) and $t_{(6)}$ = 0.02, $p$ = 0.972 in **g** ($n$ = 8 mice). (**h**) Schematic diagram illustrating the implantation of the microdialysis probe in the mediobasal hypothalamus. (**i**) GLP1 concentrations in the ARH interstitial liquid collected by microdialysis every 15 minutes following i.p. liraglutide (t0 min) injection (0.1 mg/kg) in control ($n$ = 6) and GLP1R$^{tanKO}$ mice ($n$ = 5). Two-way ANOVA followed by a Bonferroni *post hoc* test, p=0.0088. AUC, one-tailed t-test, $t_{(9)}$ = 2.10, $p$ = 0.0323. Data are expressed as means ± SEM. *$p$ < 0.05; ** $p$ < 0.01, control saline vs. control liraglutide and control vs. *Glp1r*$^{tanycyteKD}$;; † $p$ < 0.05 control liraglutide vs. *Glp1r*$^{tanycyteKD}$ liraglutide.